Japan Geoscience Union Meeting 2013
(May 19-24 2013 at Makuhari, Chiba, Japan)

SMP44-01 会場:102A 時間:5 月 20 日 09:00-09:15

機械的粉砕による斜長石ガラスの構造変化
Structural change of plagioclase glasses by mechanical milling

白井　擁 [1], 奥野 正幸 [2*], 奥寺 浩樹 [2]
Yo Shirai[1], Masayuki Okuno[2*], Hiroki Okudera[2]

[1] 金沢大学大学院自然科学研究科, [2] 金沢大学理工研究域自然システム学系
[1]Kanazawa University, [2]Kanazawa University

斜長石 ($NaAlSi_3O_8$-$CaAl_2Si_2O_8$) 組成の融液は、マグマを構成する主要成分である。その組成のガラスの粉砕による構造変化の情報は、地震やマグマ活動に伴う斜長石組成の物質の構造や物性を考えるうえで非常に重要である。また、その構造についての詳しい情報は新しい珪酸塩ガラス粉末材料の開発のために有効である。珪酸塩ガラスは、加熱や圧縮だけでなく機械的粉砕によっても、そのナノ構造や密度が変化することが知られている。例えば、SiO_2 ガラスは、粉砕によりその構造中の Si-O-Si 角の減少ならびに SiO_4 四面体の 4 員環や 3 員環の増加が密度増加を引き起すと報告されている [1]。また、Albite($NaAlSi_3O_8$) 組成ガラスについても、同様の研究が行われ SiO_2 ガラスとは異なった粉砕挙動をしめすことが分かっている。本研究では、Anorthite(An100) 及び Ab50An50 組成ガラス構造の粉砕による変化を粒度分析、X 線回折及び赤外分光測定により明らかにし、既に報告されている Ab100 組成ガラスの結果を含め、斜長石ガラスの組成変化に伴う粉砕挙動の変化について考察した。

An100 及び Ab50An50 組成ガラスを溶融急冷法により作成し、ボールミルを用いて 500 時間までの粉砕実験を行った。得られたガラス試料について、粒度分析、X 線回折及び赤外分光測定を行った。約 20〜80 時間までの粉砕では、ガラスの見かけの平均粒径は約 2 μ m まで減少し、その後再び増加した。また、An100 ガラスが最も容易に粉砕されることを明らかにした。また、長時間の粉砕により見かけの平均粒径はすべてのガラスで増加し、これはガラス粒子の再凝集によるものと考えられ、その程度は Ab100 ガラスが最も強い。これらの結果は、Ab100 ガラスの構造単位が、An100 ガラスより大きいことと関係するものと思われる。

ガラスの XRD パターンは回折角約 22〜26 °付近に First Sharp Diffraction Peak (FSDP) を示す。このピーク位置は、基本構造単位の大きさに関係し、大きな値を持つほど小さい構造単位を含むことを示す。このピークの位置は、粉砕に伴いより高角度側にシフトし、その構造単位が減少することを示す。例えば、粉砕前の Ab100 組成ガラスは、TO_4 四面体 (T=Al/Si) の 6 員環を主とする構造 [2] であるが、粉砕により、より小さい 4 及び 3 員環の構造が増加したと考えられる。また、An100 ガラスの粉砕前の FSDP 位置は、Ab100 ガラスより大きい。これは、An100 ガラスの基本構造単位が 4 員環であること [2] に関係し、その粉砕によるピークシフトが Ab100 ガラスに比べて小さいことは、粉砕による構造変化が小さいことを示している。また、SiO_2 及び Ab100 ガラスについて粉砕による密度増加が報告されている [2] ことから、An100 及び Ab50An50 ガラスも粉砕によりその密度が増加していると考えられる。しかし、An100 ガラスのピークシフトが Ab100 ガラスより小さいことから、粉砕による密度増加は Ab100 ガラスのほうが大きいと考えられ、これは粉砕前の構造の違いが原因と思われる。ただし、Ab50An50 ガラスの変化は三つのガラスで最も大きく、密度変化も大きいものと思われる。また、すべてのガラスで 10 時間までの粉砕では、FSDP 位置はほとんど変化しないことから、10 時間程度の粉砕では、内部構造の変化は非常に小さいものと思われる。

赤外分光測定の結果から、800cm^{-1} 付近のバンドは、T-O-T 結合に関係している。このバンドの強度は、粉砕に伴い減少する。しかし、その減少程度は Ab100<An100<Ab50An50 の順であり、Ab50An50 ガラスで大きく減少する。このことは、粉砕により Ab50An50 ガラスが最も激しく構造を変化させることを意味し、FSDP の粉砕による変化と矛盾しない。

以上、斜長石ガラスは、粉砕によりその基本構造単位が減少し、密度が増加するものと考えられる。また、Ab50An50>Ab100>An10 の順で構造の変化が大きいことを明らかにした。この変化は、粉砕による長石ガラス中の Na^+ 及び Ca^{2+} イオンを中心としたユニットの形成に起因している可能性がある。

References
[1] Iwao, M and Okuno, M., Koyano, M. and Ktayama, S. (2010) J. Min. Petrol. Sci., Vol. 105, 135-141
[2] Okuno, M. and Marumo, F. (1982) Mineralogical Journal, Vol.11, 180-196

キーワード: 斜長石ガラス, ボールミル, ナノ構造, X 線回折, 赤外分光
Keywords: plagioclase glass, ball mill, nano-structure, X-ray diffraction, IR spectroscopy

Japan Geoscience Union Meeting 2013
(May 19-24 2013 at Makuhari, Chiba, Japan)

SMP44-02 会場:102A 時間:5 月 20 日 09:15-09:30

高圧におけるパイロープメルトの Al の配位数について
X-ray diffraction analysis of pyrope melts at high pressures

横田 育美[1], 浦川 啓[1*], 亀卦川卓美[2]
Ikumi Yokota[1], Satoru Urakawa[1*], Takumi Kikegawa[2]

[1] 岡山大学自然科学研究科, [2] 高エネ研・フォトンファクトリー
[1]Dept Earth Sci, Okayama Univ, [2]KEK PF

固液分離は地球内部の化学進化の主要なメカニズムである。地球内部におけるメルトの移動は，その粘性と密度によってコントロールされる。これらのメルトの物性はマグマの構造と密接に関連している。そのため、高圧におけるマグマの構造は地球惑星内部のマグマの関連した現象を解明する上で重要な研究課題である。珪酸塩メルトの急冷ガラスは急冷・脱圧時の構造緩和の影響を避けられないため，高圧下のメルトの構造研究にはその場観察が必須である。本研究では高温高圧 X 線回折からパイロープ組成メルトの構造の圧力変化について調べた。本研究で着目したパイロープは Filed Strength（Z/r）が高い Mg を含むため，配位数の高い Al を含む傾向が強い。

高圧実験は KEK，PF で MAX80 を用いて 5.5GPa･2300K までの条件で行った。出発試料は 1 気圧で作成した $Mg_3Al_2Si_3O_{12}$ 組成のガラスを用いて，グラファイトカプセルに封入した。メルトの回折実験は融点から 50～100K 高温側で，白色 X 線を使ったエネルギー分散法で行った。回折プロファイルから干渉関数を導き、フーリエ法で解析した。

パイロープメルトの動径分布関数 D(r) の 4 配位の Al-O と Si-O に対応する第一ピーク（～1.7 Å）の圧力変化に注目すると，圧力に伴いピーク強度が減少した。一方，1.9 Å付近のでは強度の増加が認められる。これは，高圧ほど Al の配位数が増加して Al-O 距離が伸びていることと対応していると考えられる。TO_4 四面体を構成する Al と Si の配位数が増加するためには非架橋酸素が存在することが要求される。NBO/T の大きいパイロープ組成（Mg3Al2Si3O12）では非架橋酸素を多く含まれるため，配位数増加が顕著であると考えられる。

キーワード: マグマ, 放射光, 高圧
Keywords: magma, synchrotron radiation, high pressure

Japan Geoscience Union Meeting 2013
(May 19-24 2013 at Makuhari, Chiba, Japan)

SMP44-03 会場:102A 時間:5 月 20 日 09:30-09:45

Forsterite-$MgSiO_3$ 液体界面の構造と物性
Structure and properties of forsterite-$MgSiO_3$ liquid interface

則竹 史哉 [1*], 河村　雄行 [1]
Fumiya Noritake[1*], Katsuyuki Kawamura[1]

[1] 岡山大学
[1]Okayama University

Knowledge about viscosities and permeability of partial molten rocks is important to understand the thermal history of the Earth and volcanism. For understanding those obtained by experiments and estimating the physical properties at extreme conditions that difficult to reproduce in laboratory experiments, knowledge about structure and properties of silicate crystal-liquid interfaces is necessary. In this study, structure and properties of the forsterite-$MgSiO_3$ liquid interface are investigated by using molecular dynamics simulations. It is essential to know the structure and physical properties of forsterite-$MgSiO_3$ liquid interfaces since forsterite is the liquidus mineral of primordial magmas.

Molecular dynamics simulations were performed with NPT ensemble using MXDORTO code. The interatomic potential model used in this study is same with used in Noritake et al. (2012). The initial structure is 21440 atom system in which a sheet of $MgSiO_3$ liquid consist of 8000 atoms is sandwiched between (010) surfaces of forsterite and 43440 atom system in which a sheet of $MgSiO_3$ liquid consist of 30000 atoms is sandwiched between (010) surfaces of forsterite. Structure and properties in the vicinity of interface was obtained at 0.1 MPa and various temperatures.

From simulation results, characteristic structure was observed in the forsterite-$MgSiO_3$ liquid interface. In the crystal-liquid interface, 2-30% of SiO4 tetrahedra of forsterite surface bridge SiO_4 tetrahedra in liquid. In liquid region, SiO_4 tetrahedra concentrate in the vicinity of surface and form an SiO_4 tetrahedra rich layer of 0.4 to 0.6 nm thickness. Inner side of the first SiO_4 rich layer in $MgSiO_3$ sheet in liquid, the Mg rich second layer of 0.6 nm thickness is formed. Consequently, the structure of liquid is different from that of bulk liquid in 1.2 nm from crystal-liquid surface. However, the biased concentration approaches to bulk composition with the distance from the interface. In the first layer, internal energy of the system is lowered by bridging between SiO_4 tetrahedra at the crystal-liquid interface, and Coulombic interaction between non-bridging oxygen in liquid and magnesium at the crystal surface. In the second layer, interaction between concentrated magnesium and excess oxygen by bridging lower the internal energy.

The 2D self-diffusion coefficient oxygen in the plane in first layer is a half order lower than that of bulk liquid. However, The 2D self-diffusion coefficient of oxygen in Mg-rich second layer is a half order higher than that of bulk liquid. Existence of bridging oxygen between crystal and liquid, and concentration of SiO_4 tetrahedra in first layer might decrease the self-diffusion coefficient of oxygen in the first layer. Concentration of free oxygen, non-bridging oxygen and magnesium might increase the self-diffusion coefficient of oxygen in second layer.

This simulation results suggest that existence of small amount of melt might considerably decrease the viscosities of partial molten rocks and considerably increase permeability of partial molten rocks. However, it should be confirmed that this double layered structure in forsterite-$MgSiO_3$ liquid interface is equilibrium by performing of long time calculations.

キーワード: 界面, 分子動力学計算, 珪酸塩, 結晶, 液体
Keywords: Interface, Molecular dynamics simulation, Silicates, Crystal, Liquid

Japan Geoscience Union Meeting 2013
(May 19-24 2013 at Makuhari, Chiba, Japan)

SMP44-04 会場:102A 時間:5 月 20 日 09:45-10:00

温度勾配場におけるマントルオリビンの化学的不均質形成
Chemical heterogeneity in mantle olivine by temperature gradient

安居 俊紀 [1*], 近藤 忠 [1]
Toshinori Yasui[1*], Tadashi Kondo[1]

[1] 大阪大学大学院理学研究科
[1]Graduate School of Science, Osaka Univ

Laser-heated diamond anvil cell (LHDAC) has been used as a major method to generate high temperature and pressure conditions of the Earth's interior. In the laser heating experiments,only a local region can be raised to high temperature with a strong temperature gradient in the sample. The Soret effect is known as a phenomenon of chemical diffusion induced by temperature gradient, which causes a change of homogeneous material to heterogeneous chemistry. While the Soret diffusion in liquids has been popularly studied, that in solids and its pressure dependence have not been studied well because the Soret effect is relatively slow and more complex in solids than in liquids. The previous experiments using LHDAC (Heinz & Jeanloz 1987, Sinmyo & Hirose 2010, etc.) reported that a steep temperature gradient makes a large difference of element concentration between the laser-heated spot and its edge, however, the Soret effect in LHDAC have not been quantitatively analyzed.

In this study, we studied the material experienced a steep temperature gradient using LHDAC. Single-crystal or powdered San Carlos olivine with the composition of $(Mg_{0.89},Fe_{0.11})_2SiO_4$ was used as the starting material. The single-crystal experiments were conducted with NaCl as a pressure medium, while we loaded no pressure medium in powder experiments. Each sample was heated using a Nd:YAG laser without moving laser spot and kept the same temperature gradient. Temperature profile was measured by a spectroradiometric method. The recovered samples were analyzed using Field Emission-Scanning Electron Microscope (FE-SEM) and Electron Probe Microanalysis (EPMA). Experimental pressure and temperature were 10-30GPa and 1000-2000K, heating duration was 10-120 minutes. Various chemical heterogeneity formation was observed in different experimental conditions such as temperature gradient, heating duration and phase transition. We will report the details of these results on the Soret diffusion.

キーワード: レーザー加熱型ダイヤモンドアンビルセル, ソーレ効果, 固体内拡散
Keywords: LHDAC, Soret effect, diffusion in solid

Japan Geoscience Union Meeting 2013
(May 19-24 2013 at Makuhari, Chiba, Japan)

SMP44-05 会場:102A 時間:5 月 20 日 10:00-10:15

Zn_2GeO_4 スピネル相と Zn_2SiO_4 変形スピネル相の結晶構造
Crystal structures of Zn_2GeO_4 spinel and Zn_2SiO_4 modified spinel phases

神崎 正美 [1*], 薛 献宇 [1]
Masami Kanzaki[1*], Xianyu Xue[1]

[1] 岡山大学地球物質科学研究センター
[1]Inst. Study Earth's Interior, Okayama U.

マントル高圧鉱物と関連して、Zn_2GeO_4 と Zn_2SiO_4 の高圧相関係について 60-70 年代に調べられたが (e.g., Syono et al., 1971)、高圧相の結晶構造については Zn_2SiO_4 II 相以外は調べられていない。昨年の会議では Zn_2SiO_4 の III と IV 相の構造を報告した (SIT02-24)。本講演では、Zn_2GeO_4 の立方晶と正方晶スピネル相、Zn_2SiO_4 の V 相の結晶構造について報告し、加えて。Zn_2SiO_4 の III と IV 相について新しく分かった構造的な知見についても触れる。

試料は全て 5000 トン川井型マルチアンビル高圧装置で合成し、急冷回収したものである。粉末 X 線回折パターンは SPring-8 BL19B2 にて大型デバイ・シェラーカメラで測定した。構造精密化はリートベルト法 (RIETAN-FP) で行った。解析の詳細は Kanzaki and Xue (2012) と同じである。V 相については ^{29}Si MAS NMR 測定を行った。

Zn_2GeO_4 の立方晶と正方晶スピネル相はそれぞれ 3 GPa, 1600 ^{o}C, 5 GPa, 1200 ^{o}C で合成した。両相はこれまでの予想どおり、４配位席を亜鉛が占める逆スピネル型であった。正方晶スピネルでは、Zn と Ge の八面体席での秩序化により対称性が下がっている。これは Zn_2TiO_4 と同構造である。I.D. Brown の bond valence 計算法を使った結合距離の計算は、測定結果とよく一致した。

Zn_2SiO_4 の III, IV 相の構造 (Liu et al., 2013) については昨年の要旨に出ているが (SIT02-24)、その後 III 相については構造が $(Zn_{1.1}Li_{0.6}Si_{0.3})SiO_4$ 高温相と同じであることが分かった。この種のオリビン構造の６配位席を占める原子が４配位席に移動した構造を Baur(1980) は tetrahedral olivine と呼んだ。IV 相については、２個の ZnO_4 と１個の SiO_4 が１つの酸素を共有する tricluster が c 軸方向につながってコラムを作っている。同様なコラムは II 相にも存在し、II 相と IV 相の近い密度を説明する。

V 相が変形スピネル構造を持つことは以前から指摘されていたが (Syono et al., 1971)、今回の解析で確認された。構造は Mg_2SiO_4 wadsleyite とほぼ同じであり、Zn は八面体席のみを占めており、Zn と Si の disorder はない。これは ^{29}Si MAS NMR で１つの４配位 Si ピークが見られたことと一致する。

Baur, W.H., Inorg. Nucl. Chem. Lett., 16, 525-527, 1980
Kanzaki, M. and Xue, X., Inorg. Chem., 51, 6164-6172, 2012
Liu, X., Kanzaki, M. and Xue, X, Phys. Chem. Mineral., submitted
Syono, Y., Akimoto, S., and Matsui, Y., J. Solid State Chem., 3, 369-380, 1971

キーワード: Zn2SiO4, Zn2GeO4, 高圧相, 結晶構造, スピネル, 結晶化学
Keywords: Zn2SiO4, Zn2GeO4, high pressure phase, crystal structure, spinel, crystal chemistry

Japan Geoscience Union Meeting 2013
(May 19-24 2013 at Makuhari, Chiba, Japan)

SMP44-06 会場:102A 時間:5 月 20 日 10:15-10:30

ペロブスカイト型NaZnF3、NaMnF3の高圧相転移と、MgSiO3アナログ物質としてのポストペロブスカイト型A+B2+F3
High-Pressure Transitions of NaZnF3 and NaMnF3 Perovskites with Implication to MgSiO3 Postperovskite Analogues

赤荻 正樹[1*], 白子雄一[1], 永仮貴之[1], 糀谷浩[1], 遊佐斉[2], 山浦一成[2]
Masaki Akaogi[1*], SHIRAKO, Yuichi[1], NAGAKARI, Takayuki[1], KOJITANI, Hiroshi[1], YUSA, Hitoshi[2], YAMAURA, Kazunari[2]

[1] 学習院大理, [2] 物材機構
[1]Dept. Chem., Gakushuin University, [2]Nat. Inst. Mater. Sci.

MgSiO3 を主成分とするペロブスカイト (Pv) 相のポストペロブスカイト (pPv) への転移は下部マントル最深部で起きているとされ、pPv 型 MgSiO3 の性質を明らかにすることはコアーマントル境界領域の構造とダイナミクスを解明するために重要である。しかしこの転移が 120GPa、2000 ℃を越える超高圧高温下で起こることや pPv 相が常圧に戻すとアモルファス化することから、より低圧で同じ転移を起し、常温常圧に pPv 相が回収できる ABX3 化合物の探索とその構造、物性の研究が意義を持つと考えられる。近年、著者らは約 20GPa 以下の圧力で Pv ― pPv 転移を起こす ABX3 化合物として、CaRuO3、CaRhO3、NaNiF3、NaCoF3 を新たに発見し、高圧相関係の決定、Pv、pPv 相の精密構造解析、物性測定などを行ってきた (Kojitani et al., 2007, Shirako et al., 2009, 2012, Yusa et al., 2012)。今回、新たに NaZnF3、NaMnF3 ペロブスカイトの高圧相転移を調べ、相関係の決定、NaZnF3 Pv, pPv 相の構造精密化を行った。また NaNiF3、NaCoF3 の結果と合わせて、フッ化物 A+B2+F3 が MgSiO3 の良いモデル物質になりうることを議論する。

マルチアンビル装置を用い 9-24 GPa、600-1100 oC において NaZnF3、NaMnF3 Pv の相転移実験を行った。常圧に回収された NaZnF3 試料は液体窒素中で粉末化した後、粉末 X 線回折装置で相の同定を行った。NaMnF3 では高圧合成された焼結体試料を微小部 X 線回折装置で調べた。また NaZnF3 pPv の粉末 X 線回折データを用い、リートベルト法により構造を精密化した。

NaZnF3 Pv は約 10 ― 15GPa で pPv に転移した。常圧回収された NaZnF3 試料は単相の pPv ではなく、一部が Pv に戻っていた。その Pv ― pPv 転移の相境界線は、P(GPa) = 4.9 + 0.011T(oC) と決定され、体積変化は― 1.9 %であった。NaMnF3 Pv は約 8 ― 12GPa で Na3Mn2F7 相と MnF2 相に分解した。その回収試料で MnF2 相は?PbO2 型構造であったが、高温高圧下では O-I 型またはコチュナイト型であったと考えられる。リートベルト解析により精密決定された常圧での NaZnF3 pPv 構造は NaNiF3 pPv 構造に近く、両者の八面体は CaMO3 pPv（M =白金族元素、Sn）の八面体より変形が小さく、120GPa での MgSiO3 pPv（Murakami et al., 2004）のそれに近い。NaZnF3, NaNiF3, NaCoF3 はいずれも 20GPa 以下で Pv ― pPv 転移を起こし、体積変化は― 1~2 %、相境界線の勾配は 10-15MPa/℃である。またこれらのフッ化物 Pv、pPv の a, b, c 軸の圧縮率の大小関係は MgSiO3Pv、pPv と同じであり、圧力によって Pv 八面体の回転角が 26 °付近まで達すると、pPv へ転移する。以上のことから、これらのフッ化物は、MgSiO3 の Pv ― pPv 転移の低圧での良いモデル物質になると考えられる。特に NaNiF3 は pPv 相が単相で常圧回収できる点で、モデル物質として有用である。

キーワード: ペロブスカイト, ポストペロブスカイト, 高圧相転移, フッ化物, 下部マントル, アナログ物質
Keywords: perovskite, postperovskite, high-pressure transition, fluoride, lower mantle, analogue material

Japan Geoscience Union Meeting 2013
(May 19-24 2013 at Makuhari, Chiba, Japan)

SMP44-07 会場:102A 時間:5 月 20 日 11:00-11:15

Ab initio computation on the Fe L-edge X-ray emission spectroscopy of Fe-bearing MgSiO3

Ab initio computation on the Fe L-edge X-ray emission spectroscopy of Fe-bearing MgSiO3

Xianlong Wang[1*], Taku Tsuchiya[1]
Xianlong Wang[1*], Taku Tsuchiya[1]

[1]Geodynamics Research Center,Ehime University
[1]Geodynamics Research Center,Ehime University

Behaviors of iron (Fe) in the minerals of the Earth's lower mantle (LM), including valence state, spin state, and chemical environments, at high pressures are important for more detailed understanding the LM properties. The pressure induced spin transition of Fe-bearing MgO and $MgSiO_3$ perovskite (Pv) were detected of usually by using high-resolution K-edge X-ray emission spectroscopy (XES) [1,2,3] and confirmed by theoretical simulations [4,5]. Since the Fe K-edge XES is associated to the 3p orbital, which is far from the valence orbitals (3d and 4s), it provides no information about Fe's coordination environments. However, Fe L-edge XES can directly determine the distribution and intensity of Fe-3d character. To identify the spin state, valence state and substitution site of Fe in Fe-bearing Pv at the LM pressure range, we systematically investigated the L-edge XES of Fe^{2+}- and Fe^{3+} (Al^{3+})-bearing Pv under high pressure by using the first-principles method combined with the slater-transition method. Our results show that the spin transition of Fe^{2+} and Fe^{3+} can be identified easily by the L-edge XES technique. The valence state of Fe can be furthermore certified, since the shift of the first main peak of Fe^{3+} is about two times larger than that of Fe^{2+} across the spin transition. The width of the L-edge XES of Fe^{3+} is also sensitive to the substitution site, indicating that their coordination environments might also be distinguishable from the Fe L-edge XES spectra. These strong sensitivities to the Fe states suggest that the high-resolution Fe L-edge XES measurement would be a useful experimental technique to investigate Fe-bearing silicate minerals. Corresponding experiments are expected.

キーワード: First-principles calculation, First-principles calculation, Fe L-edge XES, Mg perovskite
Keywords: First-principles calculation, First-principles calculation, Fe L-edge XES, Mg perovskite

Japan Geoscience Union Meeting 2013
(May 19-24 2013 at Makuhari, Chiba, Japan)

SMP44-08 会場:102A 時間:5 月 20 日 11:15-11:30

$Ca_2MgSi_2O_7$-$Ca_2Fe^{3+}AlSiO_7$ 系合成メリライトの高圧下における放射光 X 線回折及びメスバウアー分光に関する研究
Synchrotron XRD and Mossbauer spectroscopic study on $Ca_2MgSi_2O_7$-Ca_2Fe^{3+} series melilite at high pressures

浜田 麻希 [1*], 大谷 栄治 [1], 三井 隆也 [2], 増田 亮 [2], 赤坂 正秀 [3]
Maki Hamada[1*], Eiji Ohtani[1], Takaya Mitsui[2], Ryo Masuda[2], Masahide Akasaka[3]

[1] 東北大, [2] 日本原子力研究開発機構, [3] 島根大
[1]Tohoku Univ., [2]JAEA, [3]Shimane Univ.

Synthetic $Ca_2MgSi_2O_7$ (akermanite: Ak)-Ca_2Fe^3+$AlSiO_7$ (ferrialuminium gehlenite: FAGeh) series melilites were investigated using synchrotron X-ray diffraction and synchrotron-radiation-based Mossbauer spectroscopic methods to determine the distribution of Fe^{3+} between two structurally independent tetrahedral sites (T1 and T2), and the relationship between ionic substitution and incommensurate structure in melilite at high pressures. ^{57}Fe-doped Ak-FAGeh melilites were synthesized from starting material with composition of $Ak_{50}FAGeh_{50}$ by sintering technique at 1140-1180 oC and 1 atm for high pressure experiment. The average chemical composition of the synthetic melilites was $Ca_{2.00}Mg_{0.56}Fe^{3+}{}_{0.42}Al_{0.44}Si_{1.57}O_7$. The site populations at the T1 and T2 sites at the synthetic condition were determined by X-ray Rietveld analysis and 57Fe Mossbauer spectroscopy (340MBq ^{57}Co source) to be $[0.557Mg+0.280Fe^{3+}+0.237Al]_{T1}$ $[0.197Fe^{3+}+0.176Al+1.574Si]_{T2}$ (apfu: atoms per formula unit), which is consistent with that by Hamada and Akasaka (in press).

The experiments at high pressures were performed using a diamond anvil cell (DAC) with culet size of 0.3 mm. A Rhenium gasket was pre-indented to 0.06 mm in thickness, and a hole with 0.1 mm in a diameter was drilled in the gasket as the sample chamber. NaCl was used as pressure medium. In addition to the powder sample, several ruby tips (0.01-0.02 mm in diameter) were put into the chamber as a pressure marker. The pressure was estimated based on Ruby fluorescence (Mao et al., 1978). Mossbauer spectra and X-ray diffraction were taken at the beamline BL11XU of SPring-8. The energy of used gamma-ray for Mossbauer spectroscopy was 14.4125 keV. Mossbauer spectra were measured at 0.8, 1.6, 14.1, 18.7 GPa. The spectra were fitted to Lorentzians with widths and intensities constrained to be equal at each site, using synchrotron-based-Mossbauer analysis program S8QBMOSS (Hamada and Akasaka, in prep.).

At 0.8 and 1.6 GPa, Mossbauer spectra consisted of two doublets assigned to T1 and T2 sites. However, Isomer Shifts (*I.S.*) of T1 and T2 sites at 1.6 GPa (0.11(5) and 0.05(5) mm/s, respectively) were smaller than those at ambient condition. Area ratio of Fe^{3+}(T1):Fe^{3+}(T2) at ambient condition was 47(1):53(2) (Hamada and Akasaka, in press). Whereas, area ratio at 0.8 and 1.6 GPa were 52(10):48(9) and 44(9):56(8), respectively. Mossbauer spectra at 14.1 and 18.7 GPa consisted of only one doublet assigned to Fe3+ at T2 site. However, the half width was broad, suggesting that the spectrum consists of strongly superimposed doublets.

The variation of the Mossbauer hyperfine parameters (*I.S.* and quadrupole splitting *Q.S.*) suggests that covalencies of T1-O and T2-O bonds increase and difference of geometric properties (site distortion and mean T-O distance) between $T1O_4$ and $T2O_4$ tetrahedra becomes smaller with increasing pressure. Yang et al. (1997) reported the incommensurate (IC)-normal (N) phase transition at 1.7 GPa. The smaller *I.S.* values may be caused by IC-N phase transition.

キーワード: 放射光 X 線回折, 放射光メスバウアー分光分析, 合成メリライト, 変調構造, 高圧
Keywords: Synchrotron X-ray diffraction, Synchrotron Mossbauer spectroscopy, Synthetic melilite, Incommensurate structure, High pressure

Japan Geoscience Union Meeting 2013
(May 19-24 2013 at Makuhari, Chiba, Japan)

SMP44-09 会場:102A 時間:5 月 20 日 11:30-11:45

(Mg,Fe)O の常圧下における磁気相図の再考
Magnetic phase diagram of (Mg,Fe)O: reinvestigation

藤井 敦大 [1*], 近藤 忠 [1], 谷口 年史 [1]
Atsuhiro Fujii[1*], Tadashi Kondo[1], Toshifumi Taniguchi[1]

[1] 大阪大学大学院理学研究科
[1]Graduate School of Science, Osaka Univ.

(Mg,Fe)O shows complex magnetic behavior due to the presence of non-magnetic magnesium ion. For example, $(Mg_{0.23}Fe_{0.77})_{0.92}O$ shows Neel transition at 128 K and spin-glass like phenomena below 76 K at ambient pressure [Abbas and Hicks, 1990]. Although we reported a magnetic phase diagram and suggested that the magnetic structure would be differ between iron-rich side and magnesium-rich side [Fujii et al. 2011], the magnetic property of (Mg,Fe)O at ambient pressure is still unclear. In this study, we reexamined the compositional dependence of magnetic ordering of (Mg,Fe)O at ambient pressure. We used Superconducting Quantum Interference Device (SQUID) magnetometer (MPMS-7 or MPMS-XL, Quantum design Inc.) to measure the temperature dependence of magnetic susceptibility by cooling sample in zero field (ZFC) and in a field (FC). The magnetic field dependent of susceptibility and the temperature dependence of AC magnetic susceptibility were newly measured. In the iron-rich (Mg,Fe)O, the ZFC curve show a peak-like cusp at relatively high temperature and a kink at low temperature. An irreversibility was observed between the ZFC curve and FC curve below the kink temperature. These behaviors are the same as those of $(Mg_{0.23}Fe_{0.77})_{0.92}O$ observed in the previous study [Abbas and Hicks, 1990]. Therefore, the kink and the cusp would indicate a spin-glass transition and Neel transition, respectively. In the case of the magnesium-rich (Mg,Fe)O, the ZFC curve show no kink and an irreversibility below the cusp temperature. Therefore, it would show no Neel transition but spin-glass transition. We also observed a superparamagentic like phenomena in all sample. These interpretations are supported by the magnetic field dependence of susceptibility and the AC magnetic susceptibility measurement. Therefore, the magnetic ordering of magnesium-rich (Mg,Fe)O is distinctly different from iron-rich (Mg,Fe)O at ambient pressure.

キーワード: (Mg,Fe)O, 磁気秩序
Keywords: (Mg,Fe)O, magnetic ordering

Japan Geoscience Union Meeting 2013
(May 19-24 2013 at Makuhari, Chiba, Japan)

SMP44-10 会場:102A 時間:5 月 20 日 11:45-12:00

フォルステライトのカソードルミネッセンスにおける温度消光メカニズム
Temperature quenching mechanism of cathodoluminescence in forsterite

西戸 裕嗣 [1*], 遠藤太郎 [1], 蜷川清隆 [1], 鹿山雅裕 [2], アーノルド　グチック [3]
Hirotsugu Nishido[1*], Taro Endo[1], Kiyotaka Ninagawa[1], Masahiro Kayama[2], Arnold Gucsik[3]

[1] 岡山理科大学, [2] 広島大学, [3] 東北大学
[1]Okayama University of Science, [2]Hiroshima University, [3]Tohoku University

Recently, cathodoluminescence (CL) zoning of the forsterite in carbonaceous meteorites has been investigated to clarify the origin and thermal history of the chondrules. CL spectroscopy can detect a trace amount of impurity Recently, cathodoluminescence (CL) zoning of the forsterite in carbonaceous meteorites has been investigated to clarify the origin and thermal history of the chondrules. CL spectroscopy can detect a trace amount of impurity elements such as Mn, Cr and Ti and lattice defects, which relate to Al-O centers and primary intrinsic centers. However, a small amount of divalent Fe ions as quencher easily eliminate CL emissions caused by any luminescent centers, so only near end forsterite could emit CL. In this study CL spectroscopy of forsteric samples has been conducted to interpret emission mechanism of their luminescent centers by an SEM-CL, and quantitatively analyze a thermal effect on forsterite CL by assuming the Mott-Seitz quenching model.

Forsterite crystals (Fo: 99.1) in basalt from Mogok, Myanmar and micro-grains (Fo: 99.7-99.8) in chondrules from Allende and Kaba meteorites classified as a CV3 were prepared for CL spectral measurements. CL spectroscopy was made by a SEM-CL system, which is comprised of SEM (JEOL: JSM-5410) combined with a grating monochromator (OXFORD: Mono CL2) at accelerating voltage of 15 kV and beam current of 1.0 nA in a beam scan mode. The sample temperature was controlled by flowing liquid nitrogen and using an embedded heater in a cryostage. All spectra were corrected for total instrumental response, which was determined using a calibrated standard lamp.

At room temperature, the CL spectra show broad emission bands at around 400 nm in blue region and at around 650 nm in red region, and pronounced emissions increasing to IR region with small emissions at around 720 nm. These bands can be assigned to structural defect, divalent Mn and trivalent Cr impurities, respectively. Their emission intensities increase with a decrease in sample temperature. In general, luminescence efficiency decreases with rising temperature due to an increase in non-radiative transitions, which has been known as temperature quenching.

CL spectral peaks in energy unit were deconvoluted by Gaussian curve fitting to determine the emission component for each emission center. The emission peak in blue region can be separated into two components centered at 3.15 and 2.99 eV, and the peaks caused by Mn and Cr impurity centers can be fixed at 1.91 and 1.74 eV, respectively. By assuming the Mott-Seitz model, activation energy in each temperature quenching process can be calculated by Arrhenius plots using integral intensity of each component. The straight-line relationships in the plots resulted in each activation energy as follows; blue emission at 3.15 eV: 0.08-0.04 eV, blue emission at 2.99 eV: 0.10-0.05 eV, red emission at 1.91 eV: 0.01-0.005 eV, red emission at 1.74 eV: 0.01-0.02 eV. The values of activation energies for blue emissions caused by structural defects correspond to the vibration energy of Si-O stretching mode in the lattice, and the values for red emissions caused by Mn and Cr impurity centers to Mg-O vibration energy. It suggests that the temperature quenching energy might be transferred as a phonon to the specific lattice vibration.

キーワード: フォルステライト, カソードルミネッセンス, 温度消光
Keywords: forsterite, cathodoluminescence, temperature quenching

Japan Geoscience Union Meeting 2013
(May 19-24 2013 at Makuhari, Chiba, Japan)

SMP44-11 会場:102A 時間:5 月 20 日 12:00-12:15

共振法によるクロミアンスピネルの単結晶弾性定数の測定
Measurements of elastic constants of single-crystal chromian spinel by fequency resonant ultrasound spectroscopy

小野 謙弥 [1*], 原田 裕也 [2], 米田 明 [3], 山本 順司 [4], 渡辺 了 [1]
Kenya Ono[1*], Yuya Harada[2], Akira Yoneda[3], Junji Yamamoto[4], Tohru Watanabe[1]

[1] 富山大学大学院, [2] 広島大学大学院, [3] 岡山大学地球物質科学研究センター, [4] 北海道大学総合博物館
[1]Department of Earth Sciences, University of Toyama, [2]Department of Earth and Planetary Systems Science, Faculty of Science, Hiroshima University, [3]Institute for Study of the Earth's Interior, Okayama University, [4]Hokkaido University Museum, Hokkaido University

Chromian spinel grains in mantle xenoliths usually contain fluid inclusions whose residual pressure (fluid density) can provide us the origin depth of the xenoliths. Elastic properties of chromian spinel are essential for precise estimation of the origin depth. Although elastic constants of spinel ($MgAl_2O_4$) and chromite ($FeCr_2O_4$) have been already reported, few studies have been done on chromian spinel. We thus have studied elastic constants of a chromian spinel single-crystal via a resonance method.

Chromian spinel grains were collected from mantle xenoliths from Sveyagin, Russia (Yamamoto et al., 2009, Island Arc). One grain was selected in terms of the uniformity of crystallographic orientation examined by SEM-EBSD. The selected grain was shaped into a rectangular parallelepiped (0.517x0.417x0.412mm^3). Each face was polished flat ($<$ 1 micrometer) in an orientation perpendicular to $\{100\}$ or $\{110\}$. The crystallographic orientation of the specimen was determined by the X-ray precession method. The density is 3.83(1) x 10^3 kg/m^3, which is calculated from the chemical composition analyzed with EPMA and the lattice parameter (a= 0.8115(1) nm) determined by XRD.

Lower 16 oscillation modes were observed in the frequency range from 4 to 9 MHz. The oscillation of a specimen is not free oscillation, because the specimen is held between two transducers. A specimen-holding force F affects resonance frequencies. In order to infer the resonance frequencies of free oscillation, resonance frequencies were measured as a function of the specimen-holding force F and then extrapolated to F=0.

Elastic constants are determined by comparing calculated and measured resonance frequencies. FEM was employed to calculate resonance frequencies. C_{11}, C_{12} and C_{44} are 264(3), 154(3), and 142.6(2) (GPa), respectively. Compared with elastic constants of end members, spinel (Yoneda, 1990) and chromite (Hearmon, 1990), chromian spinel has the lowest C_{11} and intermediate C_{12} and C_{44}.

キーワード: 弾性定数, クロミアンスピネル, 共振法, マントル捕獲岩
Keywords: elastic constants, chromian spinel, resonance method, mantle xenoliths

Japan Geoscience Union Meeting 2013
(May 19-24 2013 at Makuhari, Chiba, Japan)

SMP44-12 会場:102A 時間:5 月 20 日 12:15-12:30

三次元顕微蛍光分光測定によって可視化されるサファイヤ中の包有物の残留圧力分布
Three dimensional visualization of residual pressure around inclusions in sapphire

鍵 裕之 [1*], 亀形 菜々子 [1], ジョセリン フエンテ [1], 野口 直樹 [1], 阿依アヒマディ [2]
Hiroyuki Kagi[1*], Nanako Kamegata[1], Jocelyn Fuetes[1], Naoki Noguchi[1], Ahmadjan Abduriyim[2]

[1] 東京大学大学院理学系研究科, [2] アメリカ宝石学協会
[1]Graduate School of Science, University of Tokyo, [2]Gemological Institute of America

Mantle derived minerals can tell us much information about processes within the deep Earth. It is important to determine the original depth of these mineral samples. Kagi et al. 2009 showed that three-dimensional Raman mapping observations can be used to visualize the distribution of residual pressure around inclusions in diamond, which has provided information about the depth of diamond formation. Corundum is the second hardest mineral after diamond and is expected to also show substantial residual pressure around inclusions.

Samples were collected from New South Wales, Australia as well as Chanaburi, Thailand and are associated with alkali basalts. It is possible to distinguish between corundum crystals formed from various settings, such as metamorphic versus igneous settings, based on trace element analyses. However, distinguishing between crystals of different geographic locality and similar geologic settings is not yet possible using nondestructive methods. Based on current geochemical observations, there are two models for the formation of igneous corundum crystals. Guo et al. 1996 proposed that these crystals formed in the middle crust by a hybrid reaction between carbonatite melt and silicic magma. Alternatively, Sutherland et al. 1998 suggested that they may form directly from volatile-rich felsic melts generated at lower crustal conditions. By using 3D mapping techniques, it may be possible to evaluate the P-T history of the host rock as well as differentiate between gems from different localities.

The fluorescence spectrum of corundum has two peaks associated with the excitation of Cr^{3+} impurities in its structure, R1 and R2. Because the R2 line is insensitive to differential stress, the residual pressure can be calculated based on the peak shift of the R2 line using a pressure calibration curve.

The samples were excited using 514.5 nm emission of Ar-ion laser with a diameter of 2 micron. Measurements were taken every 5 to 10 micrometers around albite, zircon, and rutile inclusions using a point-by-point mapping illumination system. The R2 and R1 lines of the fluorescence spectra were fitted by Lorentzian functions after subtraction of background. In order to account for peak oscillations caused by changes in room temperature, real-time calibration of the fluorescence spectra energy axes were performed by neon emission lines as discussed in Odake et al. 2008.

Over 25 two- and three-dimensional maps of various inclusions have been created so far. The maximum residual pressure for each map ranges from 0.1 GPa to 0.51 GPa. In many of these samples, stress distribution can be explained by differences in elastic constants between the host and inclusion. For example, our results show one slice of a 3D map around a zircon inclusion. In this case, the c-axis of the corundum and the c-axis of the zircon are nearly parallel. With decreasing temperature and pressure, the c-axis is expected to have higher residual pressure due to differences in linear thermal expansion coefficients and bulk moduli between the host and inclusion. It is clear that the c- axis has the highest residual pressure, as expected. Another notable observation is that the maximum residual pressure surrounding zircons correlates with length of the crystal along the c-axis. Two distinct trends between residual pressure and length are observed. This may be due to many factors including the relative orientation of the host and inclusion or the presence of cracks surrounding the inclusion. It could also be due to the different geographic localities. However, more measurements need to be taken to confirm.

Previous methods to determine original depth, such as those used by Barron 2005 and Izraeli et al. 1999, which assume isotropic elastic properties in inclusion and diamond, cannot be used in these corundum-inclusion pairs. Our results show that relative orientation of corundum and inclusions must be accounted for in future calculations of P-T history.

キーワード: 残留圧力, 蛍光スペクトル, ルビー, サファイヤ, 包有物
Keywords: residual pressure, fluorescence spectra, ruby, sapphire, inclusions

Japan Geoscience Union Meeting 2013
(May 19-24 2013 at Makuhari, Chiba, Japan)

SMP44-P01 会場:コンベンションホール 時間:5 月 20 日 18:15-19:30

第一原理計算による硫化ヒ素分子の構造多様性
Ab initio quantum chemical investigation of arsenic sulfide molecular diversity

興野 純 [1*]
Atsushi Kyono[1*]

[1] 筑波大学大学院生命環境系地球進化科学専攻
[1]Div. of Earth Evolution Sci., Grad. Sch. of Life & Environmental Sci., Univ. of Tsukuba

The structural diversity of arsenic sulfide molecules in compositions between As_4S_6 and As_4S was investigated using ab initio quantum chemical calculations. The As_4S_6 molecule consists of four trigonal pyramid coordinations of As atoms bonding to three S atoms. In the As_4S_5 composition, only one type of molecular configuration corresponds to an uzonite-type molecule. In the As_4S_4 composition, two molecular configurations exist with realgar-type and pararealgar-type molecules. Three molecular configurations are in the As_4S_3 composition. The first configuration comprises trigonal pyramidal As atom coordinations of two types: bonding to two S atoms and one As atom, and bonding to one S atom and two As atoms. The second is the molecular configuration of dimorphite. The third comprises trigonal pyramidal As atom coordinations of two types: bonding to three As atoms, and bonding to one As atom and two S atoms. The As_4S_2 composition allows molecular configurations of two types. One is comprised of trigonal pyramidal As atom configurations of one type bonding to two As atoms and one S atom. The other comprises trigonal pyramidal As atom coordinations of three types: bonding to two S atoms and one As atoms, bonding to one S atom and two As atoms, and bonding to three As atoms. The As_4S molecule has trigonal pyramidal As atom coordinations of two types: bonding one S atom and two As atoms, and bonding to three As atoms. The As_4S composition permits only one molecular configuration, which suggests that the mineral duranusite comprises the As_4S molecular geometry. In all, ten molecular configurations are predicted in the molecular hierarchy of the arsenic sulfide binary system. The simulated Raman spectral profiles are helpful in searching for undiscovered arsenic sulfide minerals.
Keywords: arsenic sulfide minerals, molecular configuration, diversity, hierarchy, ab initio quantum chemical calculation

Japan Geoscience Union Meeting 2013
(May 19-24 2013 at Makuhari, Chiba, Japan)

SMP44-P02 会場:コンベンションホール 時間:5 月 20 日 18:15-19:30

高圧下におけるクリストバライトへのヘリウムの固溶による体積及び結晶構造変化
Volume and crystal structure change due to He incorporation into cristobalite at high pressures

松井 正典[1*], 佐藤 友子[2], 船守 展正[3]
Masanori Matsui[1*], Tomoko Sato[2], Nobumasa Funamori[3]

[1] 兵県大理, [2] 広大理, [3] 東大理
[1]School of Sci., Univ. of Hyogo, [2]Dept. of Earth and Planetary Systems Sci., Hiroshima Univ., [3]Dept. of Earth and Planetary Sci., Univ. of Tokyo

我々は最近、ダイヤモンドアンビルセルを用いた放射光高圧 X 線回折実験に基づいて、室温高圧下でシリカガラスにかなり多量のヘリウムが固溶する（10 GPa で SiO2 の 1 モルあたり He が 1 モル以上）こと、及びその際に、圧縮率が劇的に減少することを見出した（Sato et al., 2011; Shen et al., 2011）。続いて、シリカガラスと一部同様な構造を持っていると考えられているクリストバライトについても、同様に、室温高圧下で多量の He が固溶することを見出した（Sato et al., 2012）。クリストバライトー He の系については、圧縮により、8 GPa 付近で新たな相が生成すること（cristobalite-He I と呼ぶ）、及び cristobalite-He I を 15 GPa 付近から減圧すると、7 GPa 付近で別の新たな相が生成すること（cristobalite-He II と呼ぶ）を見出した（Sato et al., 2012）。我々は今回、第一原理計算に基づいて、cristobalite-He I と II の両相について、それらの結晶構造と圧縮挙動、エネルギー的安定性、He 含有量を検討し、実測の X 線回折データと比較したのでそれらの結果を報告する。

計算は VASP（Kresse and Furthmuller, 1996）を使用し、密度汎関数法に基づく第一原理バンド計算を行った。電子構造計算は PAW 法（Blochl, 1994）を、また電子の交換相関項については GGA 法（Perdew et al., 1996）を用いた。結晶の対称性（空間群）については、それぞれ実測あるいは仮定したものに固定して計算を行った。まず、クリストバライト（空間群 P41212）とクリストバライト II（P21/c）、及び He（P63/mmc）について、それらの構造と構造の圧力依存、エネルギー的安定性を計算により求め、可能な実測データ（Dove et al., 2000; Dera et al., 2011; Mao et al., 1988）と比較した。その結果、格子定数、原子間距離、角度とも、極めて良い精度でそれぞれの実測データが再現できることを確かめた。このことは、今回の第一原理計算が、クリストバライトー He の系に充分適用できることを示すものであろう。

クリストバライトは室温下で 1.5 GPa 付近でクリストバライト II に相転移する（Palmer and Finger, 1994; Dove et al., 2000 など）。ゆえに、まず He が高圧下でクリストバライト II の格子に、空間群を保持した状態で（P21/c, Z = 8）固溶すると仮定して計算を開始した。He の初期座標については、クリストバライト II の構造中の大きな空隙に配置すること、また、He の含有量については、SiO2 の 1 分子あたり、0.5 モル及び 1.0 モルの He が固溶する 2 つのモデルを考えた。それぞれについて、いくつか可能な構造モデルを試み、それらのうち最もエンタルピーが小さいものを最終モデル（それぞれ model 1、model 2 と呼ぶ）として採用した。model 1 と 2 の構造は、Si と O 原子位置については、互いに良く似ていること、加えて、両モデルの平均構造をとると、得られた構造（model 3 と呼ぶ）から求められる d 値と X 線回折強度が、Sato et al.(2012) が 8 GPa 以上の高圧下で見出した cristobalite-He I の実測 X 線回折データを極めて良く再現することを確認した。また、計算に基づく減圧過程で、model 2 が菱面体格子を持つ構造に相転移する（model 4 と呼ぶ）こと、及び model 4 が、Sato et al.(2012) が減圧過程で見出した cristobalite-He II の実測の X 線回折データを極めて良く再現できることを確認した。

キーワード: クリストバライト, ヘリウム, 高圧, 結晶構造, 相転移
Keywords: cristobalite, helium, high pressure, crystal structure, phase transition

Japan Geoscience Union Meeting 2013
(May 19-24 2013 at Makuhari, Chiba, Japan)

SMP44-P03 会場:コンベンションホール 時間:5 月 20 日 18:15-19:30

Mg2Si2O6-CaMgSi2O6-CaFeSi2O6-Fe2Si2O6 系高温常圧における高温型斜方輝石の安定領域
Stability of Orthopyroxene in pyroxene quadrilateral at 1 atm and High Temperatures

大井 修吾 [1*]
Shugo Ohi[1*]

[1] 京都大学理学研究科
[1]Graduate School of Science, Kyoto University

輝石は火成岩に広く出現する造岩鉱物であり、変成岩、地殻深部、隕石においてもきわめて重要な鉱物である。Enstatite (En, Mg2Si2O6) ― diopside (Di, CaMgSi2O6) 系において、1400 度付近で安定領域を持つ斜方輝石 (Opx) 相が 1970 年代から注目され続けてきた。Ohi et al. (2008) は、低温型斜方輝石 (LT-Opx) から高温型斜方輝石 (HT-Opx) への転移を観察し、1000 度以下で安定領域を持つ Opx は LT-Opx、1400 度付近で安定領域を持つ Opx は HT-Opx であることを示した。

Fe を含まない系においては HT-Opx の安定領域は明らかにされたが、Fe を含んだ場合における安定領域はまだ知られていない。本研究では、En?Di- hedenbergite (Hd, CaFeSi2O6)- ferrosilite (Fs, Fe2Si2O6) 系における LT-Opx と HT-Opx の安定領域を明らかにし、LT-Opx と HT-Opx を区別した輝石台形を完成させることを目的としている。今回の発表では、En-Di 近傍の HT-Opx の安定領域が、Fe を含むことによりどのように変化するのかを、合成実験により明らかにした。

合成実験は、Ca : Mg : Fe = 0.03-0.15 : 0.92-0.65 : 0.05-0.20 の範囲の組成を持つ 6 種類のゲルを出発物質に用い、1180・1280・1345・1375 度の温度で、3-14 日間行った。雰囲気制御は、H2-CO2 混合ガスで p(O2) をバッファーし、IW 雰囲気で実験を行った。

回収した試料は、粉末 X 線回折実験 (XRD: RIGAKU, SmartLab) で相同定し、走査型電子顕微鏡+エネルギー分散 X 線分光装置 (SEM-EDX: HITACHI S-3000H + HORIBA EMAX7000) で組成分析を行った。また必要に応じて、SEM に付属の後方散乱電子回折 (EBSD) 検出器 (HKL, CHANNEL5) を用いて相同定を行った。今回の合成実験で晶出する相は、単斜エンスタタイト (Cen: プロトエンスタタイト相の急冷で生成)・Opx・ピジョン輝石 (Pig)・Di が予想できるが、XRD では Cen と Pig を区別することはできなかった。そのため、XRD の同定では、Cen と Pig をまとめて Ca-poor Cpx と表記する。

1180 度の実験で得られた試料は粒径が 5um 以下のものがほとんどであり、SEM-EDX による組成分析を行うことができなかった。XRD の結果はいずれの合成試料でも、Ca-poor Cpx and/or Di

であり、Opx は認められなかった。1280 度の実験では、5um 程度の粒径を持つ試料があり、組成分析ができる試料があった。SEM-EDX による組成分析の結果、Ca0.06Mg1.84Fe0.10Si2O6 の組成を持つ Opx が同定された。また、XRD の結果、En : Fs = 9 : 1 よりも Fe 含有量の多い試料で、Opx を観察することができた。1345 度、1370 度の実験では、10um 以上の粒径を持つものが多かった。SEM-EDX 及び EBSD による組成分析・相同定の結果、Cen、Opx、Pig、Di が観察できた。Opx と Pig が共存する時、２相の間の化学組成に優位に差が見られなかったため、この２相の間の不混和領域は、非常に狭いことが予想される。

Fe を含まない En-Di 系においては、LT-Opx は 1005 度以上、HT-Opx は 1370 度以下では晶出しない (Carlson, 1988)。本研究では、1180 度では Opx が観察できなかったが、1280 度以上の温度で観察できたため、今回観察した Opx は全て HT-Opx であることがわかった。また、Fe を含まない場合 1370 度以下では晶出しない HT-Opx が、1280-1375 度では観察できたため、HT-Opx は Fe を含むほど低温まで安定領域を持つことがわかった。Pig の安定領域も、Fe を含むほど低くなることが知られており、HT-Opx この傾向は Pig の場合と同じである。

Keywords: orthopyroxene, high temperature, enstatite-diopside-hedenbergite-ferrosilite system, phase transition

Japan Geoscience Union Meeting 2013
(May 19-24 2013 at Makuhari, Chiba, Japan)

SMP44-P04 会場:コンベンションホール 時間:5 月 20 日 18:15-19:30

Thermal equation of state of manganite
Thermal equation of state of manganite

鈴木 昭夫 [1*]
Akio Suzuki[1*]

[1] 東北大学大学院理学研究科地学専攻
[1]Tohoku University

Manganese(III) oxide hydroxide is found in nature as the minerals groutite (alpha-MnOOH), feitknechtite (beta-MnOOH), and manganite (gamma-MnOOH). Manganite is one of the naturally occurring polymorphs of Mn3+OOH with an InOOH-related structure. The oxide hydroxides of trivalent cations have an InOOH-related structure, in which the trivalent cation is octahedrally coordinated by oxygen. InOOH, beta-CrOOH, epsilon-FeOOH, and delta-AlOOH have orthorhombic unit cells. However, manganite is monoclinic because of the Jahn?Teller distortion. Here we report the pressure?volume-temperature relation of gamma-MnOOH. The aim of this study was to determine the compression behavior of an oxide hydroxide with an InOOH-related structure.

The high-pressure X-ray diffraction study was carried out at the station NE7A at the Photon Factory Advanced Ring (PF-AR) in High Energy Acceleration Research Organization (KEK). The PF-AR operates at 6.5 GeV with an injection current of 60 mA. We used a Kawai-type multianvil apparatus driven by a large volume press, MAX-III. Tungsten carbide cubes (Tungaloy grade F) of 22 mm edge length were used for high-pressure generation.

Experiments were performed up to a pressure of 18.0 GPa and a temperature of 700K. The pressure?volume data were fitted by a third-order Birch?Murnaghan equation of state with the following parameters: V_0 = 135.22(8) A^3, K_0 = 77(2) GPa and K_{0T} = 12.0(5). The temperature dependence of the bulk modulus was determined to be dK/dT= -0.022(6) GPa/K. This study shows that the most compressible axis is the b-axis. The beta angle in the monoclinic unit cell decreases with increasing pressure.

キーワード: X線回折, 状態方程式, 高圧力, MnOOH, 放射光, 含水鉱物
Keywords: X-ray diffraction, Equation of state, High pressure, MnOOH, Synchrotron radiation, Hydrous mineral

Japan Geoscience Union Meeting 2013
(May 19-24 2013 at Makuhari, Chiba, Japan)

SMP44-P05 会場:コンベンションホール 時間:5 月 20 日 18:15-19:30

高温 X 線回折測定と高圧ラマン測定に基づく SiO2 スティショバイトと MgSiO3 アキモトアイトの熱膨張率の決定
Thermal expansivities of stishovite and akimotoite by high-pressure Raman and high-temperature X-ray diffraction methods

山崎 萌波 [1*], 糀谷 浩 [1], 赤荻 正樹 [1]
Monami Yamazaki[1*], Hiroshi Kojitani[1], Masaki Akaogi[1]

[1] 学習院大学理学部化学科
[1]Dept. Cemistry, Gakushuin Univ

SiO_2 スティショバイトや $MgSiO_3$ アキモトアイトは、マントル深部に沈み込んだ海洋プレートや大陸地殻の構成物質であろうと考えられている。どちらの物質とも、常圧で一定温度以上に加熱するとその構造を保てないため 1 気圧高温下での熱膨張率の測定が困難であり、未だに精度良く決定されていない。本研究では、高圧ラマン測定結果に基づく格子振動モデル計算と高温粉末 X 線回折測定により、SiO_2 スティショバイトとイルメナイト型 $MgSiO_3$ の熱膨張率を決定した。

高圧合成した SiO_2 スティショバイトと $MgSiO_3$ アキモトアイトについて、ダイヤモンドアンビルセル高圧発生装置と顕微ラマン分光装置を用いて、高圧ラマン測定を常圧から 10 GPa の範囲で行った。ラマンピーク位置の圧力依存性から各振動モードのモードグリューナイゼンパラメーターを決定し、それらの荷重平均から熱力学的グリューナイゼンパラメーター (γ_{th}) を求めた。熱膨張率は $\alpha = C_V \gamma_{th} / K_T V$ より算出された。定容熱容量 C_V は格子振動モデル計算を用いて求められた。また、$MgSiO_3$ アキモトアイトについては、室温から 773 K の範囲で高温粉末 X 線回折測定を行い、格子体積の温度変化から熱膨張率を決定した。

$\alpha = a + bT + cT^{-1} + dT^{-2}$ の式を使い、SiO_2 スティショバイトの熱膨張率は、$a = 1.85 \times 10^{-5}$, $b = 3.25 \times 10^{-9}$, $c = -2.41 \times 10^{-3}$, $d = -1.11 \times 10^{-1}$、$MgSiO_3$ アキモトアイトの熱膨張率は、$a = 2.53 \times 10^{-5}$, $b = 7.62 \times 10^{-9}$, $c = -8.63 \times 10^{-4}$, $d = -5.51 \times 10^{-1}$ と決定された。

今回決定された SiO_2 スティショバイトの熱膨張率は、Nishihara et al. (2005) の高圧高温その場観察実験による値よりも小さいが、実験的に決められた相境界線を用いて Mao et al.(2001) により最適化された熱膨張率と調和的である。また、Nishihara et al. (2005) の熱膨張率を用いて定圧熱容量 C_P を $C_P = C_V + \alpha^2 K_T V T$ より算出した場合、Akaogi et al. (2011) の熱量測定と格子振動モデル計算による C_P を 2000 K で 5 %上回る。一方、本研究の熱膨張率から計算された C_P は、Akaogi et al. (2011) の値と良い一致を示しており、本研究で求めた熱膨張率は信頼性が高いといえる。

本研究の高温 X 線回折測定による $MgSiO_3$ アキモトアイトの熱膨張率は、Ashida et al. (1988) により同じ方法で測定された熱膨張率と調和的である。Wang et al. (2004) は高圧高温その場観察実験を用いて熱膨張率を求めた。実測値の熱膨張率と比較すると、Wang et al. (2004) の熱膨張率は小さい。この実験方法は、高圧高温での体積データを用いて常圧での熱膨張率を求めるということから大きな不確実さを伴う。本研究の高圧ラマン測定に基づいた熱膨張率は、上記の実測値と調和的であるため、1000 K 以上の熱膨張率もより信頼性が高いと思われる。よって $MgSiO_3$ アキモトアイトの熱膨張率は従来用いられてきた値よりも大きいと考えられる。

キーワード: アキモトアイト, スティショバイト, 熱膨張率, 高圧ラマン測定, 高温 X 線回折測定
Keywords: akimotoite, stishovite, thermal expansivities, high-pressure Raman spectroscopy, high-temperature X-ray diffraction measurements

Japan Geoscience Union Meeting 2013
(May 19-24 2013 at Makuhari, Chiba, Japan)

SMP44-P06 会場:コンベンションホール 時間:5 月 20 日 18:15-19:30

熱水環境下で固定化した合成オパール
The synthetic opal fixed in hydrothermal environment

山崎 悠子 [1*], 磯部 博志 [1]
Yuko Yamasaki[1*], Hiroshi Isobe[1]

[1] 熊本大学大学院自然科学研究科理学専攻
[1]Grad. Sch. Sci. Tech., Kumamoto Univ

オパールは、最も貴重なシリカ鉱物のうちの 1 つで、直径数 100nm という微小な非晶質シリカ粒子の規則正しい層状構造により可視光線が干渉を起こし、特有の遊色を示す。オパールを作る基本単位であるシリカ粒子は、オルト珪酸テトラエチル（TEOS）の加水分解による Stoeber 法によって人工的に合成することができる。しかしながら、この Stoeber 法によって生成されたシリカ粒子から、肉眼的スケールでの規則的積層構造を作り、さらに天然のオパールのように安定した構造体として固定することは難しい。本研究では、シリカ粒子集合体を熱水環境に保持することにより得られた、安定した遊色と強度を持つ合成オパールについて報告する。

Stoeber 法で作成した非晶質シリカ微粒子は、室温で沈殿させることにより高濃度の懸濁液とした。この懸濁液を、内径 6mm、高さ約 30mm の一端を閉じた石英ガラス管に、深さ約 15mm まで注入した。懸濁液を入れた石英ガラス管を、テフロン容器または耐熱合金製マイクロリアクターに封入し、100 ℃、150 ℃、200 ℃、250 ℃で、1 日から 3、10、20、30、45、75 日間保持した。このとき、飽和水蒸気圧を保持するために圧力容器に封入した蒸留水は、石英ガラス管内の懸濁液に直接触れない量に留めた。

実験開始時は白色の懸濁液であった試料は、各温度とも 1 日後には石英ガラス管底部の深さ 5mm 程度にまで沈殿していた。取り出した石英ガラス管は、室温で自然乾燥の後、構造を維持するために沈殿物表面のみを樹脂で固定した後、精密カッターを用いて縦断面を作成し実体顕微鏡および電子顕微鏡を用いて遊色組織および内部構造を観察した。

その結果、100 ℃から 200 ℃で保持した試料に、肉眼的スケールまで発達した遊色を示す領域が観察された。特に、200 ℃に保持した試料において、実験期間 5 日では赤～青色を示す比較的小さな遊色ドメインが存在しているのに対して、10 日では緑にのみ輝く、2mm を超える大きさの遊色ドメインが見られた。さらに、20 日になると上方は小さな遊色ドメインが赤～青に輝いていたが、下方は大きな遊色ドメインが見られ、緑に加え青色に輝くものが出てきた。30 日になると 5 日の試料のように小さな遊色ドメインがしかし、5 日の試料にくらべ低い密度で形成されていた。

電子顕微鏡観察の結果、遊色を示す試料においても、シリカ粒子の変形や粒間の充填物が観察された。これらの現象により、沈殿物はカッターによる切断に耐える強度を得ているものと考えられる。熱水環境は、オパールの合成過程において mm スケールを超える遊色組織の形成とその固定化に極めて大きな役割を果たしていると思われる。

キーワード: オパール, 熱水合成, 遊色組織, 非晶質シリカ
Keywords: opal, hydrothermal synthesis, opalescence domain, amorphous silica

Japan Geoscience Union Meeting 2013
(May 19-24 2013 at Makuhari, Chiba, Japan)

SMP44-P07 会場:コンベンションホール 時間:5 月 20 日 18:15-19:30

ハンレイ岩の不均一な加重による正孔電荷キャリアの発現と起電力の発生
Activation of hole charge carriers and generation of electromotive force in gabbro blocks induced by non-uniform loading

竹内 昭洋 [1*], 長尾 年恭 [1]
Akihiro Takeuchi[1*], Toshiyasu Nagao[1]

[1] 東海大学海洋研究所地震予知研究センター
[1]Earthq. Predict. Res. Cent., Inst. Ocenic Res. Dev., Tokai Univ.

When one end of vacuum-dried gabbro blocks was subjected to uniaxial loading, the unloaded end became electronically positive (+80 mV at 50-MPa). Hot point probe tests using the hot-probe with 423 K of the temperature and the cold one with 293 K found that the Seebeck coefficient of the loaded volume decreased from ˜15.8 mV/K to ˜14.9 mV/K when loaded, while the coefficient of the unloaded end did not change remarkably (˜15.6 mV/K). This means that this gabbro originally included a small number of hole charge carriers and the carriers in the loaded volume increased when loaded. From the viewpoint of the fundamental band model of solid state, the most reasonable mechanism of the increment is the decrease of the energy gap between the acceptors and the valence band top. Shear stress/strain would effectively shift the energy levels because early studies have found that the electronic conductivity of gabbro is almost independent of the hydrostatic pressure. Based on this idea, a generation model of the stress-induced electromotive force is proposed. Since this model is expected to be universally applicable to various types of rocks, similar electromotive forces in the crustal scale may be induced by seismic, volcanic, and tidal activities in the Earth and Moon.

キーワード: ハンレイ岩, 正孔電荷キャリア, 起電力, ゼーベック係数
Keywords: gabbro, hole charge carrier, electromotive force, Seebeck coefficient

Japan Geoscience Union Meeting 2013
(May 19-24 2013 at Makuhari, Chiba, Japan)

SMP44-P08 会場:コンベンションホール 時間:5 月 20 日 18:15-19:30

電子エネルギー損失分光法（EELS）による緑泥石中の鉄の二価三価比測定
Ferrous to ferric ratio measurement in chlorite using electron energy-loss spectroscopy (EELS)

井上 紗綾子 [1*], 笠間　丈史 [2], 小暮　敏博 [1]
Sayako Inoue[1*], KASAMA, Takeshi[2], Kogure, Toshihiro[1]

[1] 東大院理, [2] デンマーク工科大電顕センター
[1]Earth & Planetary Sci., Univ. Tokyo, [2]Center for Electron Nanoscopy, DTU

Determination of Fe^{3+}/Fe_{total} ratio in iron-bearing minerals is important and has been conducted using several analytical techniques such as Mosbauer spectroscopy, X-ray absorption near-edge structure (XANES) and X-ray photoelectron spectroscopy. Compared to these techniques, electron energy-loss spectroscopy (EELS) in Transmission electron microscopy (TEM) is capable of giving information of the chemical state of constituting elements in specimens, with a spatial resolution down to the nanometer scale. Detailed analysis of energy-loss near-edge structure (ELNES) of Fe-$L_{2,3}$ core-loss edges provides information about the iron oxidation state, and several methods have been proposed to quantify Fe^{3+}/Fe_{total} from the ELNES of iron (Garvie and Buseck, 1998; van Aken et al., 1998). However, because a number of silicate minerals are electron-beam sensitive, the influence of radiation damage on the quantification of Fe^{3+}/Fe_{total} by EELS should be considered. Moreover, sample preparation processes for TEM such as argon ion-milling and focused-ion-beam (FIB) milling form a damage layer on the specimen surface, which may also affect the quantification. In this study Fe^{3+}/Fe_{total} quantification in chlorite, rather beam-sensitive iron-bearing phyllosilicates, has been performed using EELS equipped to a field-emission gun TEM with a monochromator, considering the influence of radiation damage and sample conditions on the measurement.

Fe^{3+}/Fe_{total} ratios obtained from the same grain of chlorite indicated that the ratio increases significantly with the electron dose to be radiated during TEM observation and EELS acquisition, suggesting that the oxidation of iron proceeds with vitrification of chlorite by radiation. Hence, it was necessary to acquire several Fe^{3+}/Fe_{total} ratios as a function of electron dose (i.e., time) and estimate 'the damage-free ratio' by extrapolation. The surface damage layers with a thickness of several tens of nanometers, which were formed during FIB milling, are likely oxidized and therefore partially associated with the increase in the Fe^{3+}/Fe_{total} ratios.

Keywords: EELS, TEM, Phyllosilicate, Chlorite, Iron valence state, FIB

Japan Geoscience Union Meeting 2013
(May 19-24 2013 at Makuhari, Chiba, Japan)

SMP44-P09 会場:コンベンションホール 時間:5 月 20 日 18:15-19:30

紫外線と水による鉄カンラン石の変質
Change in fayalites with ultraviolet rays and water

小森 信男 [1*]
Nobuo Komori[1*]

[1] 大田区立蒲田中学校
[1]Ota ward Kamata junior high school

筆者は、紫外線と水による岩石の風化変質を実験的に調べる継続研究を中学校科学部の生徒研究として行っている。火星上に酸化鉄が多い原因の一つを明らかにするという目的のためである。このために、精製水に浸した八丈島産鉄カンラン石に紫外線を照射しその変化を調べた。火星上には、玄武岩が多く、この中には鉄カンラン石がおそらく存在する。また過去の火星上には水が存在していたと推定されている。そのため過去
の火星においては、紫外線と水が、岩石を変質させる要因の一つになったと考える。
この研究では、精製水を満たした石英試験管に１０ｇ程の鉄カンラン石を入れた。鉄カンラン石は、３～５mm程度の粒状であり、暗緑色を呈している。そして２５４ nm をピークとする紫外線を照射した。　対照実験として、同じ条件で紫外線を照射しない実験も行った。紫外線は３ヶ月照射した。なお、照射開始時の照度は４０W／m ² 程である。
紫外線を照射したものにも照射しないものにも、薄褐色の０．１mm以下の微粒子が多数生じた。この微粒子の数は、紫外線を照射したものの方がずっと多い。この微粒子は、ＥＰＭＡによる分析から、主に非晶質の水酸化鉄と考えられる。
また、紫外線を照射した方のかんらん石の表面には、１０μm前後の新鮮な穴状の構造が多数見られる。紫外線を照射しない方のかんらん石には、そのような新鮮な穴はほとんど見られない。
以上のことから、紫外線は、水に浸した鉄カンラン石の変質を促進すると考えられる。火星表面には、過去において水が存在していたことが、明らかになりつつある。火星表面においても紫外線と水によって、岩石中の鉄カンラン石の変質が促進された可能性はあると考える。

キーワード: 紫外線, 水, 鉄カンラン石, 水酸化鉄, 変質, 火星
Keywords: ultraviolet rays, water, fayalite,, iron(III) oxide, change, Mars

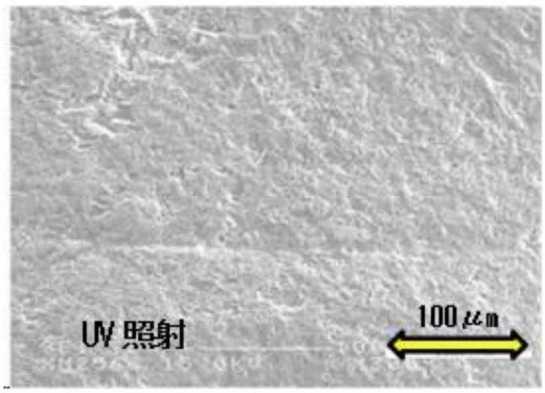

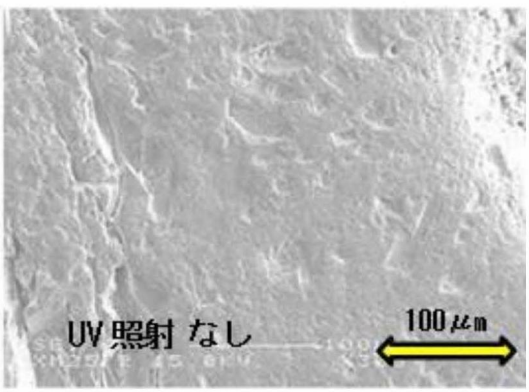

図　鉄カンラン石試料表面の電子顕微鏡写真　左：UV 照射の場合　右：UV 非照射の場合

Japan Geoscience Union Meeting 2013
(May 19-24 2013 at Makuhari, Chiba, Japan)

SMP44-P10 会場:コンベンションホール 時間:5 月 20 日 18:15-19:30

アニーリングおよび放射線効果がジルコンのカソードルミネッセンスに及ぼす影響
Annealing and radiation effects on cathodoluminescence of zircon

土屋 裕太 [1*], 鹿山 雅裕 [2], 西戸 裕嗣 [1], 能美 洋介 [1]
Yuta Tsuchiya[1*], Masahiro Kayama[2], Hirotsugu Nishido[1], Yousuke Noumi[1]

[1] 岡山理科大学生物地球学科, [2] 広島大学地球惑星システム学科
[1]Department of Biosphere-Geosphere Science, [2]Department of Earth and Planetary Systems Science

Cathodoluminescence (CL) analysis provides useful information on the existence and distribution of defects and trace elements in materials, which are related to genetic conditions such as formation temperature, metamorphic process and geochronological situation. U-Pb zircon dating (e.g., SHRIMP) is an important tool to determine geological age of a micro-ordered zircon, where CL image has been used for observation of internal zones and domains with different chemical compositions and structural disorder at spatial high resolution. CL of zircon is caused by various types of emission centers, which are divided into two groups: extrinsic center such as rare earth element (REE) and intrinsic center such as lattice defects. Above all, CL of zircon is closely related to metamorphic process and radiation from contained radionuclides. Most zircon has yellow emission, which seems to be assigned to radiation-induced defect or UO_2 centers. According to Nasdala et al. (2002) and Hancher and Hoskin (2003), the yellow emission band has been recognized to be eliminated by heat treatment. Therefore, the radiation effects on zircon CL have been studied for He^+ ion-implanted samples annealed at various temperatures to clarify radiation-induced defect centers involved with yellow CL emission in zircon.

A single crystal of zircon from Malawi (MZ) was selected for annealing and He^+ ion implantation experiments. The sliced samples were cut perpendicular to c- and a- axes, and annealed at 100 to 1400 deg. C for 12 hours. Zircon crystals in Takidani granodiorite (TZ) and Kurobegawa granite (KZ), and the sliced MZ were implanted by He^+ ion at 4.0 MeV corresponding to energy of alpha particle form ^{238}U and ^{232}Th. The radiation dose was set at 4.77×10^{-4} and 5.11×10^{-5} C/cm^2. CL spectra in the range from 300 to 800 nm with 1 nm step were measured by a scanning electron microscopy-cathodoluminescence (SEM-CL). The operating condition was set at 15 kV accelerating voltage and 0.1 nA beam current. All CL spectra were corrected for the total instrumental response.

CL spectra of untreated and annealed zircon almost show emission bands at ˜370 nm assigned to intrinsic defect center and at ˜480, ˜580 and ˜760 nm to Dy^{3+} impurity centers [Cesbron et al, 1995; Gaft et al, 2005]. Yellow CL emissions have been undetected in annealing zircons above 700 deg. C, where an elimination of radiation-induced defect centers may be appeared due to recrystallization of the structure suggested by Nasdala et al (2002). Blue CL intensity at ˜370 nm gradually increases with an increase in annealing temperature, which may be responsible for a formation of intrinsic defect center due to a recovery of the framework structure from metamict by heating. CL spectra of MZ show an increase in the yellow emission intensity with an increase in radiation dose of He^+ ion implantation as well as the emission related to the impurity centers (REE), though He^+ ion implantation reduces the intensity of impurity centers. Yellow emission intensity has a tendency to depend on radiation dose of He^+ ion implantation. TZ and KZ, with young formation ages of 1.93-1.20 Ma and 1.7-0.9 Ma, respectively [Harayama,1994; Harayama et al., 2010], show dull yellow CL emission attributed to radiation-induced defect center, suggesting relatively low radiation dose of alpha radiation from ^{238}U and ^{232}Th on them. If the component of yellow emission could be deconvoluted from the CL spectra in zircon, the intensity of yellow emission should be used for an indicator to evaluate total exposure doses on it during geological age.

キーワード: カソードルミネッセンス, ジルコン, アニーリング効果, 放射線効果
Keywords: Cathodoluminescence, Zircon, annnealing effect, radiation effect

Japan Geoscience Union Meeting 2013
(May 19-24 2013 at Makuhari, Chiba, Japan)

SMP44-P11 会場:コンベンションホール 時間:5 月 20 日 18:15-19:30

Smithsonite のカソードルミネッセンス発光メカニズム
Emission mechanism of cathodoluminescence in smithsonite

槙尾 雅人 [1*], 西戸裕嗣 [1], 草野展弘 [1], 蜷川清隆 [1]
Masato Makio[1*], Hirotsugu Nishido[1], Nobuhiro Kusano[1], Kiyotaka Ninagawa[1]

[1] 岡山理科大学
[1]Okayama Univ. Sci.

Cathodoluminescence (CL) has been widely applied in mineralogical investigation, especially for carbonates. CL of carbonates is characterized by various types of emission centers such as impurity and defect centers. Smithsonite ($ZnCO_3$) has emission centers of divalent Mn ion as activator and divalent Fe ion as quencher (Gotte and Richter, 2004). However, the defect center in smithsonite has not been investigated so far, since its emission is not so often found in carbonates. We have detected blue CL emission in smithsonite, suggesting structural defect center. In this study, we have assigned emission bands in CL spectra including defect center and clarified the mechanism of the CL in smithsonite in a wide temperature range.

Three crystals of smithsonite from San Antonio, Mexico (S-08, S-11) and Slaiman, Uzbekistan (S-17) were selected for CL measurements after carbon-coating on their polished surfaces. SEM-CL analysis was conducted using an SEM (JEOL: JSM-5410) combined with a grating monochromator (Oxford: Mono CL2) to measure CL spectra ranging from 300 to 800 nm in 1 nm steps at accelerating voltage of 15 kV and beam current of 1.0 nA. The CL emitted from the samples was collected by a photon counting method with a photomultiplier tube, and converted to digital data. All spectra were corrected for total instrumental response determined using a calibrated standard lamp. The sample temperature can be controlled in the range from -190 to 50 degree C with flowing liquid nitrogen and using an embedded heater in a cryostage (Oxford: C1003). CL color imaging was carried out with Luminoscope (ELM-3 R) consisting a cooled CCD camera by excitation voltage at10kV and beam current of 0.5 mA.

CL spectra of S-11 at room temperature show a board band at around 650 nm in red region, which can be assigned to the electronic transition from excited state of 4G to ground state of 6S corresponding to divalent Mn activator substituted for Zn ion. S-08 has a broad band at around 400 nm in blue region in its CL spectrum. Its emission might be caused by the defect center in smithsonite lattice. S-17 has also emission peaks at around 650nm in red region and 400nm in blue region. The deconvolution of the spectra in an energy unit using a Gaussian fit reveals that a red emission has two components peaked at 1.61 and 1.82 eV and a blue emission consists of two components at 3.28 and 3.82 eV. Therefore, there are at least two deferent defect centers in smithsonite, suggesting different crystal fields between them. The intensity of a blue emission decreases with an increase of sample temperature as explained by a temperature quenching theory based on an increase in the probability of non-radiative transition with the rise of temperature (Mott-Seitz model). Activation energy in each temperature quenching process can be calculated by an Arrhenius plot using integrated intensity of each component as a luminescent efficiency. It results in activation energy of 0.027 eV for component centered at 3.28 eV. This energy value corresponds to the energy of O-Zn-O bending vibration (0.024 eV: Frost et al, 2008), suggesting energy-transfer from the radiation to lattice vibration as photon. However, the intensity of a red emission is not affected by the change of sample temperature. These facts indicate that the temperature quenching mechanism might depend on the types of emission centers related to impurity or structural defect.

キーワード: スミソナイト, カソードルミネッセンス, 発光メカニズム
Keywords: smithsonite, cathodoluminescence, emission mechanism

Japan Geoscience Union Meeting 2013
(May 19-24 2013 at Makuhari, Chiba, Japan)

SMP44-P12 会場:コンベンションホール 時間:5 月 20 日 18:15-19:30

粒子画像イメージング法による火山灰の粒子径と形状の数値定義
Numerical definition of particle size and shape of volcanic ash by statistical particle image analysis method.

笹倉 大督[1*], 早内愛子[1]
Daisuke Sasakura[1*], HAYAUCHI Aiko[1]

[1] スペクトリス株式会社　マルバーン事業部
[1]Malvern Japan ,Div of Spectris Co.Ltd,.

[1] Introduction
The exact definition of particle size and shape is a factor of importance in many researches connected with several geology sciences which objections are sea sand, soil and volcanic ash. The object of this report is to describe the various methods of defining these properties and to give the result of some measurements made on volcanic ash as model sample by statistical particle image analysis.

[2] Methodology
The statistical particle image analysis is possible to obtain the significant difference evaluated result of particle size and shape information by over the ten thousand numbers of particles projection images from microscopic method. The methodology of this technique is based on the digital binary image processing technology from projection image picture of CCD camera on microscope. In each CCD camera pixels has size. The determinations of particle size and shape parameter are calculated by the particle projection images which are constructed from the number pixels in CCD camera. The most of the advantage of this method is not only possible to described numerical definition of particle analysis but also available to the diverse analysis by two dimensional correlations plot between shape parameter and particle size.

[3] Material and method
Volcanic ash sample was from the Ito Pyroclastic Flow as model sample. This sample was sieved by 5 phi mesh sieve and it was come from under the mesh to isolate small particle from bulk sample. An automated particle characterization system (Morphologi G3,Malvern Instruments) was used to evaluation of statistical particle image analysis. The observation mode was diascopic mode (Transmittance mode) . Volcanic ash sample were dry dispersed using the integrated Dry sample dispersion unit via an instantaneous pulse of compressed air, and measured using Standard Operating Procedures (SOPs) which define the software and hardware settings depending. Measurements were made in an enclosed glass plate as sample carrier, minimizing environmental exposure. The analysis generated high quality images from over ten thousands of sample particles.

[4] Result
Total number of 96,029 particles was measured. Volume based circle equivalent diameter of particle size distribution (VCED) were monomodal and 14.31(d10), 30.32(d50), 45.79(d90) in micro meter. However, the number based percentage of small particles (<3 micrometer) was 74.91%. To concerning shape distribution and shown in Fig.1. Circularity was bimodal, however aspect ratio was monomodal. Recalculation of VCED was shown Fig.2 which was shape distribution data. Represented on amount of volume based percentage , the circle like particles were 3% and the angular like particles were 64% .However , in count based percentage , circle like particles were 55% and angular like particles were 21%.

[5] Summary
This report will be more discuss about application and capability of numerical definition of volcanic ash by the statistical particle image analysis as new approach for this research area.

キーワード: 火山灰, 粒子径, 形状, 画像イメージング法
Keywords: Volcanic Ash, Pariticle size, Pariticle shape, Particle Image Analysys

SMP44-P12 会場:コンベンションホール 時間:5 月 20 日 18:15-19:30

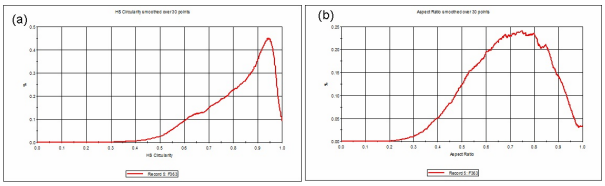

Fig.1 Shape distribution by particle image (a) Circularity (b) Aspect ratio

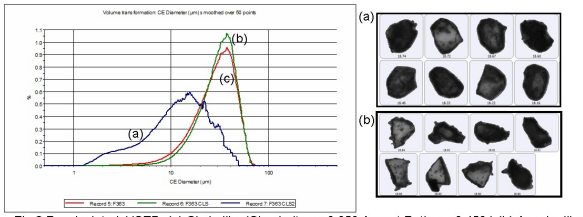

Fig.2 Recalculated VCED (a) Circle like (Circularity >= 0.850 Aspect Ratio >= 0.450) (b) Angular like (Circularity Between 0.400 - 0.750 , Aspect Ratio >= 0.450) (c) Total

Japan Geoscience Union Meeting 2013
(May 19-24 2013 at Makuhari, Chiba, Japan)

SMP44-P13 会場:コンベンションホール 時間:5 月 20 日 18:15-19:30

ドロマイトのカソードルミネッセンスにおける温度消光メカニズム
Temperature quenching mechanism of cathodoluminescence in dolomite

草野 展弘 [1*], 西戸裕嗣 [1], 槙尾雅人 [1], 蜷川清隆 [1]
Nobuhiro Kusano[1*], Hirotsugu Nishido[1], Masato Makio[1], Kiyotaka Ninagawa[1]

[1] 岡山理科大学
[1]Okayama University of Science

Cathodoluminescence (CL) has been widely applied in mineralogical and petrological investigations, especially for carbonates. Dolomite commonly red CL emission related to an impurity center of divalent Mn (Reeder , 1987; Gillhaus et al, 2001), but of which each occupancy in Ca site (A site) and/or Mg site (B site) has not been precisely estimated. Furthermore, temperature effect on CL efficiency has not been discussed in spite of potentially important function to control CL emission mechanism, though the factors effected on dolomite CL such as luminescence centers have been extensively investigated. In this study we have clarified luminescent mechanism of dolomite in a wide range of temperature using a SEM-CL, and confirmed a temperature quenching of its emissions. The quenching process has been quantitatively evaluated by CL spectral deconvolution method assuming the Mott-Seitz model, where site occupancy for Mn^{2+} ions in dolomite lattice has been also evaluated.

Three dolomite samples from Binntal/VS, Swiss (D-17a), Arizona, USA (D-26a) and New Mexico, USA (D-28a) were selected for CL measurements after carbon-coating on their polished surfaces. These samples contain Mn^{2+} ions as an activator, but too low for divalent Fe as a quencher.

SEM-CL analysis was conducted using an SEM (JEOL:JSM-5410) combined with a grating monochromator (Oxford: Mono CL2) to measure CL spectra ranging from 300 to 800 nm in 1 nm steps with a temperature controlled stage from -190 to 250 ^{o}C . The dispersed CL was collected by a photon counting method using a photomultiplier tube (R2228) and converted to digital data. All CL spectra were corrected for the total instrumental response.

All samples exhibit a broad band in red region CL spectrum between 580 and 640 nm at room temperature. The spectral peaks are sharpened and enhanced at lower temperature due to reduction of thermal lattice vibration and an increase in luminescent efficiency, suggesting high spectral resolution of the emission bands at low temperature. Therefore, a Gaussian fitting was conducted to quantitatively deconvolute spectral data obtained at low temperature in an energy unit. Two emission components at around 1.84 and 2.15 eV. The former can be assigned to the emission derived from Mn ion impurity occupied at A site, the latter to the emission at B site. The component intensities decrease in two steps of temperature range between -190 to -100 and -50 to 150 ^{o}C with an increase in sample temperature. In general, luminescence efficiency of the material decreases with a rise in temperature due to an increase in non-radiative transitions. This phenomenon has been recognized in several minerals such as quartz, cristobalite and tridymite as temperature quenching. By assuming the Mott-Seitz model, activation energy in temperature quenching process can be calculated by a Arrhenius plot using integrated intensity of each component as an emission efficiency. Each activation energy was determined as follows; 0.03 eV for A and B sites below -100 ^{o}C and 0.100 eV for A site and 0.097 eV for B site above -50 ^{o}C. The former corresponds to the value of CO_3 vibration, and the latter to Ca-O or Mg-O vibration. Judging from the similarity of the activation energy in the process of temperature quenching and lattice vibration energy, the temperature quenching energy might be transferred as a phonon to the specific lattice vibration through non-radiative transition.

キーワード: ドロマイト, カソードルミネッセンス, 温度消光
Keywords: dolomite, cathodoluminescence, temperature quenching